

Motional Resistance as Highly Selective Descriptor to Probe Dynamic Formation of Surface Films on Zinc Anode

Sangram Keshari Mohanty,^[a] Yeongin Ok,^[a] Eun Su Kim,^[a] Yuwon Park,^[b] Ji Heon Ryu,^[c] Junyoung Mun,^[b] Jeonghyeon Lee,^[d] Kyu Hyun,^[d] Madhusudana Koratikere Srinivasa,^[a] Hyein Jeong,^[a] Sri Charan Reddy,^[a] and Hyun Deog Yoo^{*[a]}

Zinc anodes are expected as a promising alternative to lithium-based anodes in energy storage systems due to their low cost, high theoretical capacity, and environmental friendliness. However, the development of efficient and stable zinc anode requires a fundamental understanding of the interfacial processes occurring during zinc deposition and dissolution cycling. In this study, we employed electrochemical quartz crystal microbalance (EQCM) analysis to investigate the potential-dependent formation and decomposition of surface films on zinc metal anodes in sulfate-based aqueous electrolytes. Changes in frequency and motional resistance served as complementary descriptors, with motional resistance being a

highly selective indicator for probing dynamic surface film formation driven by side reactions at the zinc anode. While the frequency change provided the overall changes in the mass of both zinc metal and surface films, changes in the motional resistance selectively reflected the amount and nature of the visco-elastic interface that comprise the surface films. The two descriptors provide quantitative and complementary means to discover the complex interfacial processes such as the formation of surface visco-elastic films, guiding to the development of more stable and efficient zinc-based electrochemical systems.

Introduction

Mitigating global climate change and environmental pollution requires extensive utilization of renewable energies, which is limited by the initial costs and safety concerns of the grid energy storage. In this context, there are dire research needs for developing efficient electrochemical energy storage systems (EESS) with high safety, low cost, and environmental friendliness. Although lithium-ion batteries (LIBs) dominate premium batteries' market, scaling LIBs up to a grid energy storage faces several limitations including higher cost, limited lifespan, thermal runaway, sustainability concerns, and recyclability.^[1] As an alternative, aqueous rechargeable batteries based on earth-

abundant elements are promising avenues for EESS with lower cost, higher safety, and sustainability.^[2–4] Aqueous zinc batteries (AZBs) are promising candidates for the application of large-scale energy storage owing to the advantages of low electrochemical potential (-0.76 V vs standard hydrogen electrode (SHE)), high specific and volumetric capacity (820 mAh g⁻¹ and 5855 mAh cm⁻³), benignity, and abundancy of zinc metal.^[5–10] Additionally, AZBs are further cost-effective in regards to battery manufacturing as they can be securely managed under ambient atmospheric conditions.

Alkaline electrolytes have been conventionally used for AZBs; however, they exhibit poor rechargeability due to the large active ions that prevent the reversible intercalation into the host materials and severe dendrite formation on the zinc metal anode.^[11] In this regard, mild acidic aqueous electrolytes can enhance the rechargeability of the AZBs by the simpler structure of the active ions, enabling genuine zinc-ion batteries. At the same time, mild acidic electrolytes offer potentially improved stability, safety, higher voltage, and lower cost compared to the alkaline electrolytes.^[12] To this, Yamamoto *et al.* was the first to investigate a mild acidic solution of zinc sulfate (ZnSO_4) for AZBs with high rechargeability.^[13,14] Despite the advantages over alkaline electrolytes, the ZnSO_4 electrolyte are facing various challenges that include: (1) dendrite formation on the zinc anode, which can cause short circuits and reduced cycle life, (2) surface film formation that can limit the utilization of zinc metal anode and the reversible capacity, and (3) the competing hydrogen evolution reaction (HER) that consumes zinc and reduces the overall durability and lifespan of AZBs.^[15,16] Of all the challenges, HER is at the center of the essential instability of AZBs. In acidic electrolytes, hydrogen evolution reaction (HER) (Equation 1) generates OH^- ions, which

[a] S. K. Mohanty, Y. Ok, E. S. Kim, M. K. Srinivasa, H. Jeong, S. C. Reddy, H. D. Yoo
Department of Chemistry and Institute for Future Earth, Pusan National University, Busan 46241, Republic of Korea
E-mail: hdyoo@pusn.edu

[b] Y. Park, J. Mun
School of Advanced Materials Science and Engineering, Sungkyunkwan University, Suwon 16419, Republic of Korea

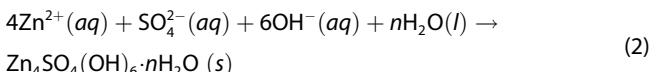
[c] J. H. Ryu
Graduate School of Convergence Technology and Energy, Tech University of Korea, Siheung 15073, Republic of Korea

[d] J. Lee, K. Hyun
School of Chemical and Biomolecular Engineering, Pusan National University, Busan 46241, Republic of Korea

 Supporting information for this article is available on the WWW under <https://doi.org/10.1002/batt.202400338>

 © 2024 The Authors. *Batteries & Supercaps* published by Wiley-VCH GmbH. This is an open access article under the terms of the Creative Commons Attribution Non-Commercial NoDerivs License, which permits use and distribution in any medium, provided the original work is properly cited, the use is non-commercial and no modifications or adaptations are made.

react with zinc to form $\text{Zn}(\text{OH})_4^{2-}$ ions that subsequently precipitate to $\text{Zn}(\text{OH})_2$ and ZnO .^[16]



In ZnSO_4 electrolytes, the Zn anode corrodes via reaction (Equation 2) that produces zinc hydroxyl sulfate (ZHS; $\text{Zn}_4\text{SO}_4(\text{OH})_6 \cdot n\text{H}_2\text{O}$), which has a significantly lower solubility product constant (K_{sp}) compared to that of $\text{Zn}(\text{OH})_2$.^[17] The passivation of the zinc can reduce the rate of anode corrosion, leading to improved stability and durability of the anode.^[15,18] Therefore, the characteristics and behavior of the surface film formed on the zinc anode in sulfate-based electrolytes need to be thoroughly investigated.

The electrochemical quartz crystal microbalance (EQCM) technique has been utilized to investigate highly sensitive interfacial phenomena, including the electrochemical deposition of zinc,^[18,19] the formation of a passivation layer within the interfacial region of substrates,^[20,21] and the sophisticated interfacial mechanism governing the (de)solvation of Li^+ ions at the electrode-electrolyte interface.^[22] EQCM analyzes the dynamics of the electrode-electrolyte interface by measuring two important parameters: the motional frequency and motional resistance. Motional frequency is pertinent to the resonant behavior of the crystal in response to a small perturbation, while motional resistance measures the damping effect of the crystal-electrolyte system caused by energy dissipation out of the viscoelastic interactions. The Sauerbrey equation ($\Delta f = -C_f \Delta m$) is commonly used for quantitative analysis of mass changes on the surface of quartz crystal resonators by the motional frequency, assuming rigid attachment and negligible thickness relative to acoustic wavelength.^[23–25] Here, Δf represents the motional frequency change, Δm is the mass change, and C_f is a constant dependent on the crystal and its mode of vibration. On the other hand, the motional resistance (ΔR_m) reflects the energy dissipation at the crystal-electrolyte interface, which is measured by analyzing the change in resonant frequency and bandwidth of the crystal. This allows for a quantitative measurement of viscoelastic energy dissipation and provides more complete description for the dynamics of the electrode-electrolyte interface.^[26,27]

Herein, we propose a complementary analytical method of monitoring mass and motional resistance to investigate the formation and decomposition of surface films by EQCM analysis during the reversible deposition and dissolution of zinc metal anodes. We found that the motional resistance change (ΔR_m) is a selective descriptor for the formation of the surface films, whereas the frequency change (Δf) represents the overall mass of both zinc metal and surface films. Our results reveal the potential-dependent and reversible formation and decomposition of surface films during the electrodeposition and dissolution of zinc in sufficiently concentrated electrolytes ($\geq 2.0 \text{ M}$). Among various concentration, the 2.0 M ZnSO_4 electrolyte concentration exhibited nearly ideal mass per electrode values

with high coulombic efficiency. The above descriptors and insights enable quantitative analysis of surface films on the zinc metal anode for developing high-performance zinc-based electrochemical systems.

Experimental

Preparation of Electrolyte and Materials

Zinc sulfate heptahydrate ($\text{ZnSO}_4 \cdot 7\text{H}_2\text{O}$; 99%; JUNSEI Co.) electrolyte solutions at concentrations of 0.1 M , 0.5 M , 1.0 M , 2.0 M , 3.0 M , and 3.2 M were prepared through the dissolution of the appropriate stoichiometric quantity of the $\text{ZnSO}_4 \cdot 7\text{H}_2\text{O}$ salt in deionized water. The resulting mixtures were stirred for a duration of 24 h to ensure thorough homogenization. A working electrode (WE) consisting of a platinum electrode attached to an AT-cut quartz crystal (Pt-QC; Neoscience Co.) was utilized, with an exposed surface area of 0.196 cm^2 . The electrode displayed a sensitivity factor of approximately $926.80 \text{ Hz} \mu\text{g}^{-1} \text{ cm}^2$. In addition to this, the WE configuration incorporated a stainless-steel plate (0.1 mm thick; SS316 L) for further analyses. The reference (RE) and counter (CE) electrodes were zinc foils (Zn; 99.98%; 0.25 mm thick; Alfa Aesar Co.) that were meticulously spot-welded to a stainless-steel plate as the current collector.

Electrochemical and Material Characterizations

A custom-designed three-electrode EQCM cell was utilized in this study, with a Pt-QC electrode as WE, and Zn foils as the RE (dimensions: $0.3 \text{ cm} \times 1 \text{ cm}$) and CE (dimensions: $0.5 \text{ cm} \times 1 \text{ cm}$). The investigation into the mass changes during zinc deposition and dissolution was carried out under room temperature and ambient atmospheric conditions. The EQCM instrument (QCA922, Seiko EG&G Co.) was integrated with a potentiostat (VMP3; Bio-Logic Co.), so that the data was measured and analyzed by EC-Lab software. During the EQCM analysis, cyclic voltammetry (CV) tests were conducted in the potential range of -0.2 V to 2.0 V vs Zn/Zn^{2+} at the scan rate of 10 mV s^{-1} .

To further analyze the deposited zinc and the byproducts, scanning electron microscopy (SEM; Regulus 8100; Hitachi Co.), energy-dispersive spectroscopy (EDS), Fourier-transform infrared spectroscopy (FT-IR; Nicolet iS50 Analytical, ThermoFisher Scientific Co.), X-ray photoelectron spectroscopy (XPS; AXIS SUPRA, Kratos Analytical Co.), and X-ray diffraction (XRD; Miniflex600; Rigaku Co.) were employed. For the materials characterizations other than XRD, a stainless-steel foil ($1 \text{ cm} \times 1 \text{ cm}$) was used as the substrate. In the case of XRD, a carbon paper (CP; $1 \text{ cm} \times 1 \text{ cm}$; MGL 190; AvCarb Co.) was the substrate for the sample preparation. The samples were prepared by scanning the potential to the desired value, followed by washing the substrate with deionized water and drying under vacuum at 60°C overnight. Pawley decomposition of the XRD patterns were made by PDXL 2 software (version 2.8.4.0; Rigaku Co.), and the diffraction patterns of ZHS with varied lattice parameters were simulated using PowderCell 2.3 software.

Viscosity Measurements

Viscosity was assessed using a rheometer (Ares G2, TA instruments) employing the DIN concentric cylinders method, while applying a range of shear rates from 1 to 100 s^{-1} . The solutions demonstrated a Newtonian fluid behavior (Figure S1). The mean viscosity was calculated by utilizing viscosity data acquired when the shear rate

was within the range of 25 to 75 s⁻¹. The viscosity measurements were conducted at a temperature of 25 °C.

Results and Discussion

Overall Scheme of this Research

The resonance frequency (Δf) of the Pt-coated piezoelectric quartz crystal (Pt-QC; Figure 1a) decreases during zinc deposition, indicating the increase in the mass according to the Sauerbrey equation (Figure 1b). At the same time, the ΔR_m increases during the zinc deposition, suggesting more hindered vibration due to the zinc deposits, surface film, or viscoelastic layer in the electrode-electrolyte interface. Conversely, during the zinc dissolution into the electrolyte, Δf increases back; however, ΔR_m continues to increase until the completion of zinc dissolution. After the completion of the zinc dissolution, ΔR_m decreases upon further elevation of the potential up to 2.0 V vs Zn/Zn²⁺. This observation suggests that surface film forms on the zinc surface during both electrodeposition and dissolution processes. Notably, the surface film persists even after the complete dissolution of zinc deposits (Figure 1c). The surface film decomposes at higher electrode potential, as supported by the simultaneous decrease in Δm and ΔR_m . The following sections will delve into the detailed EQCM behaviors of the surface films in terms of Δm , ΔR_m , and other electrochemical properties.

Electrochemical and Materials Characterization of Electrolytes

As the electrolyte concentration increased from 0.1 M to 2.0 M, the peak current of zinc dissolution increased from 0.37 to 4.25 mA cm⁻² (Figure 2a). Concurrently, there was an enhancement in coulombic efficiency by 24.9% (from 71.6% to 96.5%). Those enhancements in the electrochemical performances are deeply related to the alleviated hydrogen evolution reaction (HER) and the smaller mole fraction of the free water molecules, resulting in higher reversibility and stability of zinc metal anode.^[28]

Upon subsequent increase in the concentration to 3.2 M, the current density decreased monotonously; conversely, the coulombic efficiency showed little to no change, maintaining a similar value of 97.5% (Figure 2b). The decrease in the deposition/dissolution current can be ascribed to higher viscosity of the electrolytes at higher concentrations, which results in lower conductivity according to Walden's rule (Figures 2d and S1). Being consistent with the trends observed in the CV analysis, the 2.0 M electrolyte demonstrated the highest conductivity of 56.2 mS cm⁻¹ (Figure 2c and d). At higher concentrations, the increased ion-ion interactions led to lower ionic conductivity as represented by the lower molar conductivity according to Kohlrausch's law (Table S1).^[29] Ion-pair formation was noticeable at higher concentration, as shown by the lower slope in the molar conductivity profile; such ion-pair formation lowers the fraction of free zinc ions that can participate in ionic conduction.^[30]

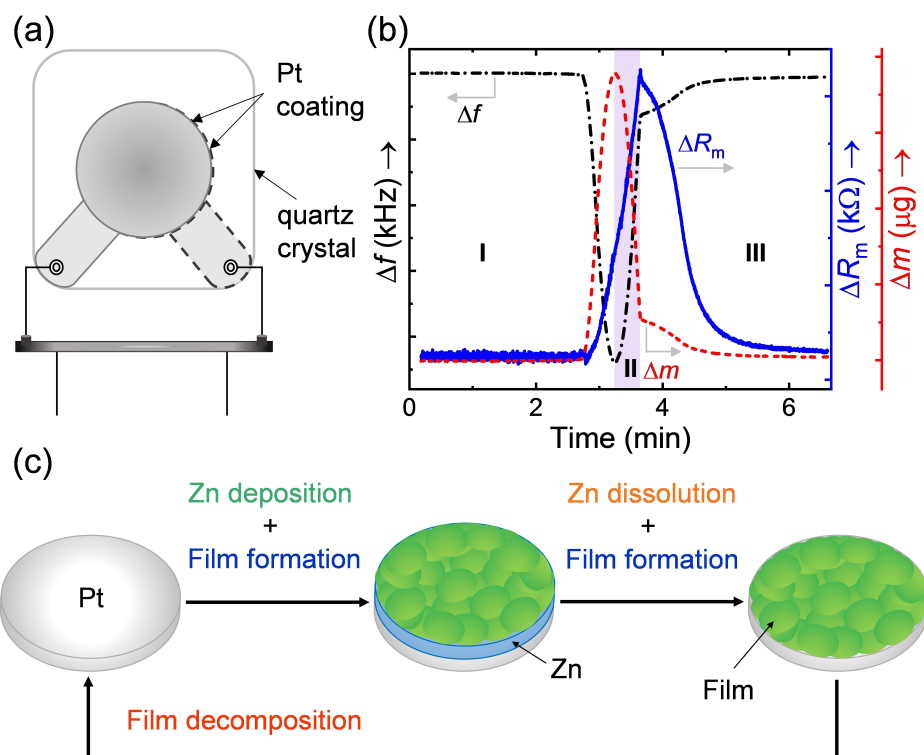


Figure 1. Scheme of the *in-situ* EQCM study of the potential dependent surface film on zinc anode by ZnSO₄ electrolyte. (a) A Pt-coated quartz crystal (Pt-QC) electrode. (b) Representative plots for the changes in vibrational frequency, mass, and motional resistance during the electrodeposition/dissolution of zinc on the Pt-QC electrode. (c) Illustration of formation and decomposition of the surface film during the deposition and dissolution of zinc in ZnSO₄ electrolyte.

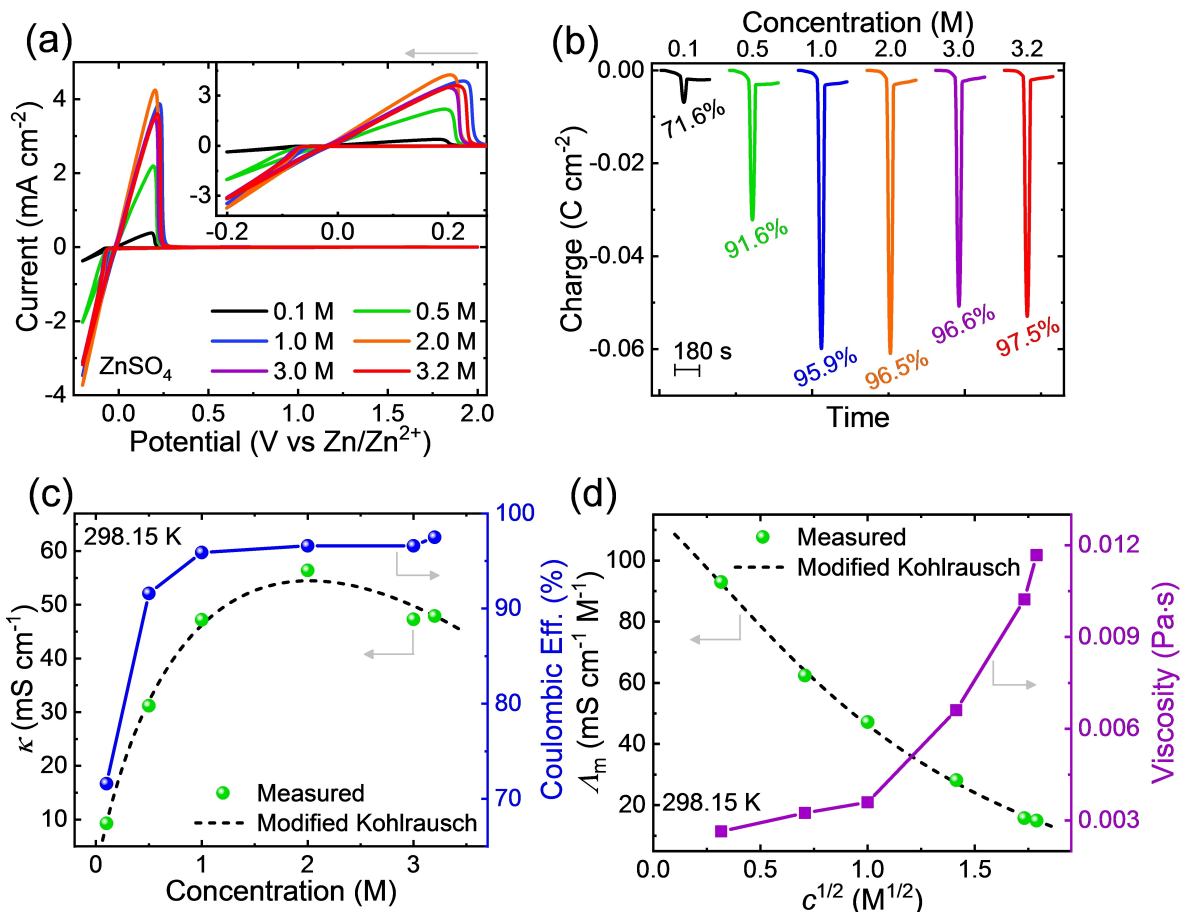


Figure 2. Electrochemical and physicochemical properties of ZnSO_4 electrolyte at varied concentrations. (a) Cyclic voltammograms and (b) the charge profiles during the zinc deposition/dissolution at varied electrolyte concentrations. (c) Conductivity, coulombic efficiency, (d) molar conductivity, and viscosity as a function of concentration at 298.15 K.

Formation of Surface Film under Different Concentrations of ZnSO_4 Electrolyte

Electrolytes with lower concentrations (*i.e.*, 0.1, 0.5 M, and 1.0 M) exhibited severe side reactions on bare Pt surface as shown by the irreversible increase in the mass upon the cathodic scan to lower potential, beginning from 1.0 V vs Zn/Zn^{2+} (Figure S2); Δm and ΔR_m did not return to their initial values during the reverse scan, indicating the irreversible formation of the reduction product. On the other hand, the Pt surface did not exhibit any significant irreversible reactions at 2.0 M or higher concentration, and the mass change was highly reversible upon the reverse scan (Figure 3b and c). This finding suggests that the electrochemical reduction of free water molecules results in the irreversible formation of byproducts in ZnSO_4 electrolyte with lower concentration.^[31] The ΔR_m quantifies the dissipation of energy as the quartz crystal vibrates in the viscoelastic media; the significant irreversibility during the reverse (*i.e.*, anodic) scans indicated the highly viscoelastic properties of the byproducts, such as lower density and rough texture of the film,^[26] in line with the highly porous morphology of zinc hydroxyl sulfate (ZHS) that is often found in the sulfate electrolytes.^[18]

The slope of Δm vs number of electrons curves (Figure 3d–f) represents the mass per electron (m.p.e.) values during the electrochemical processes. At the lower concentrations of 0.1~1.0 M, the m.p.e. values deviated from the ideal value of 32.69 g/mol_e for Zn deposition/dissolution, especially before the deposition of zinc (Figures 3d and S2). This suggested an irreversible formation of byproducts by side reactions such as HER. At 2.0 M, on the other hand, the deposition and dissolution of zinc was highly reversible and the m.p.e. was close to the ideal value (Figure 3b and e). As the concentration of the ZnSO_4 electrolyte was further increased up to 3.2 M, the slope of the deposition curve (Figures 3f and S2f) exhibited a hysteresis, especially at the end of deposition and dissolution periods. This hysteresis suggests the potential-dependent formation/decomposition of the surface film by unidentified compounds in addition to zinc deposition, possibly originated from the water-in-salt environment or the saturation of anions at the vicinity of the electrode surface.

During the reverse scan, the m.p.e. value becomes smaller than the ideal value (Figure 3f), suggesting the accumulation of ionic species during the dissolution of zinc. This phenomenon might be due to the solubility limit of the electrolytes that are highly concentrated already; this phenomenon is in line with

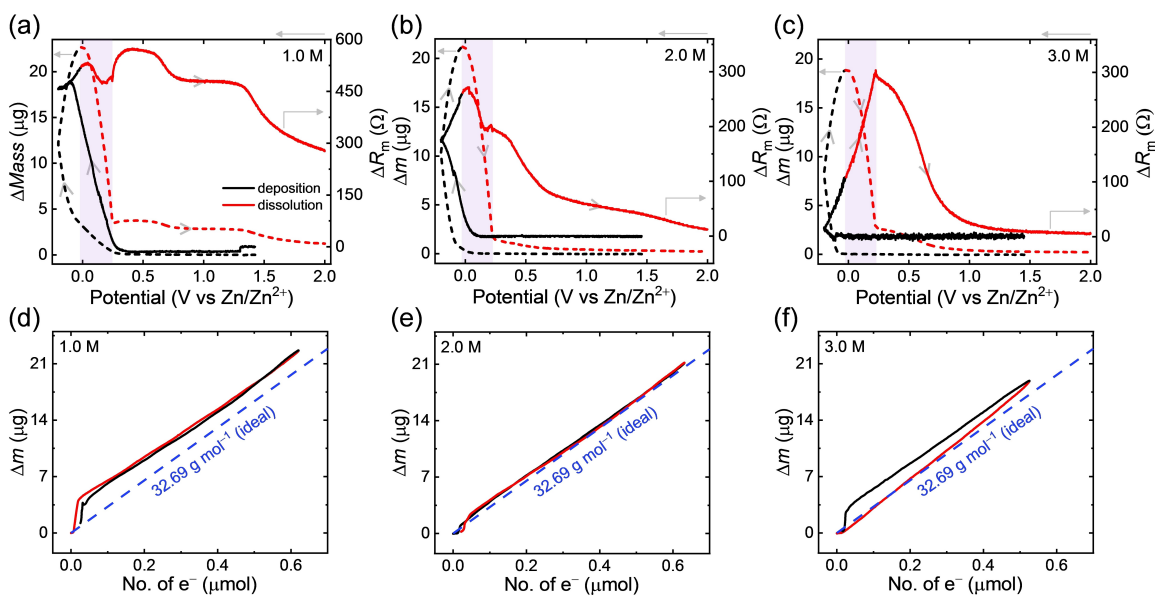


Figure 3. Electrochemical surface film dynamics: effects of ZnSO_4 concentration on the surface films during zinc deposition and dissolution. Δm and ΔR_m vs potential profiles at (a) 1.0 M, (b) 2.0 M, and (c) 3.0 M ZnSO_4 ; and the corresponding profiles of Δm vs number of electrons at (d) 1.0 M, (e) 2.0 M, and (f) 3.0 M.

the continual increase in the ΔR_m values until the completion of zinc dissolution at 0.2 V vs Zn/Zn^{2+} (Figures 3c and S2c). As the applied potential exceeded 0.2 V and reached 2.0 V vs Zn/Zn^{2+} , ΔR_m underwent a gradual reduction, ultimately converging toward zero, indicating the decomposition of the surface film. This is in line with the Δm profiles that continue decreasing to zero after the completion of the zinc dissolution. This observation suggests the reversible formation of a surface film depending on the applied potential, as shown in Figure 1. Another

important implication is that the ΔR_m selectively indicates the surface film, whereas Δm accounts for the total mass change due to the zinc deposits as well as the surface films. This special selectivity in ΔR_m can be explained by the higher viscoelastic resistance of the surface film, compared to the metallic zinc deposits with smoother and more compact morphology.

Next, we focus on the anticorrosion functionality of the surface films that mitigates the corrosion of zinc as a function of electrolyte concentration (Figure 4). As the cycling pro-

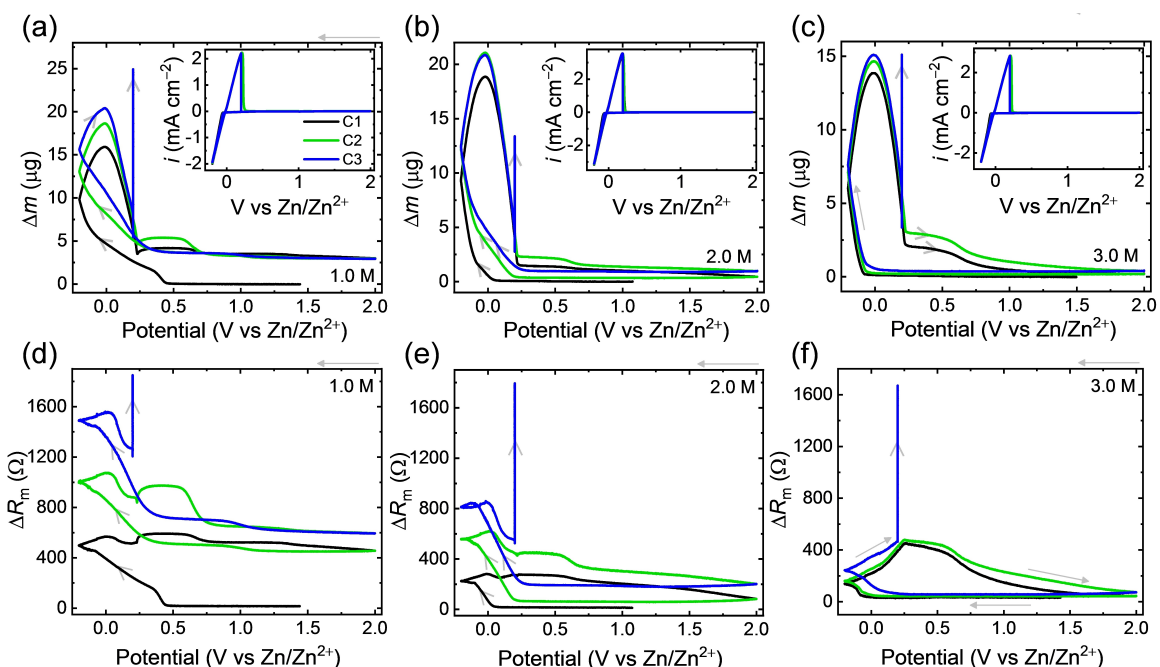


Figure 4. Δm and ΔR_m vs potential profiles during the repeated cycling in (a,d) 1.0 M, (b,e) 2.0 M, and (c,f) 3.0 M ZnSO_4 . The legends C1, C2, and C3 stand for cycle numbers.

ceeded, both Δm and ΔR_m keep increasing irreversibly in the low-concentration $ZnSO_4$ electrolytes at 0.1~0.5 M, primarily due to the continued irreversible precipitation of byproducts on the electrode surface. On the other hand, the intermediate concentration of 1.0 and 2.0 M resulted in the saturation of Δm upon cycling; however, ΔR_m persisted to increase, indicating continued change in the viscoelastic properties or morphology. The nearly saturated electrolytes at 3.0 and 3.2 M exhibited remarkable reversibility of Δm and ΔR_m (Figures 4 and S3), evidencing the excellent interfacial stability against irreversible side reactions.

It is noteworthy that these results prove the potential-dependent passivation of the zinc metal in the sulfate-based electrolytes. Holding the potential at 0.2 V vs Zn/Zn²⁺ led to a continual increase in Δm and ΔR_m (Figure 4), suggesting the continual growth of viscoelastic surface films as a function of electrode potential, not by the chemical entities such as zinc metal. Such potential-dependent formation of surface films implies that even if the films may protect zinc metal surface from various corrosion, there can be continual side reactions during the rest period. Therefore, it will be highly essential to form a genuine passivation layer to prevent the continual growth of the surface film, possibly by employing suitable additives.

During the potential hold at 0.2 V vs Zn/Zn²⁺, all electrolytes exhibited a net positive mass change (Figure 5). However, electrolytes at lower concentrations of 0.1 M and 0.5 M

exhibited a negative change in ΔR_m , which can be attributed to the formation of rigid byproducts on the electrode surface, rather than the formation of a viscoelastic film (Figures 5 and S4). The ΔR_m is nearly constant during the potential hold in 1.0 M electrolyte, whereas the ΔR_m increases in 2.0 M and higher concentrations. This observation supports that the formation of viscoelastic films become dominant in the highly concentrated $ZnSO_4$ electrolyte above 1.0 M, whereas the lower concentration prefers irreversible formation of byproducts.

Composition of the Surface Film

In general, the properties of the surface film can be ascribed to its compositions. The surface film developed on the zinc metal anode in the saturated $ZnSO_4$ aqueous electrolyte has been identified as a multifaceted blend of compounds that encompasses ZnO , $Zn(OH)_4^{2-}$, $Zn(OH)_2_3(ZnSO_4)(H_2O)_n$, and $Zn_5(OH)_6(CO_3)_2$.^[18,32,33] The exact composition of the surface film may depend on various factors such as the electrolyte concentration, pH, and potential. Surface films formed at lower concentrations of 0.1 M and 0.5 M exhibited XRD patterns of the namuwaite-type hydrated ZHS, $Zn(OH)_2_3(ZnSO_4)\cdot nH_2O$ with the hydration number (n) of 3.0~5.0 ($d_{001}\sim 10.8\text{ \AA}$) (Figures 6 and S5).^[34] At higher concentrations ($c\geq 1.0\text{ M}$), the XRD patterns match with ZHS with smaller interlayer spacing ($d_{001}\sim 7.5\text{ \AA}$), probably due to the lower number of hydration of 0.5~2.0.^[35] It

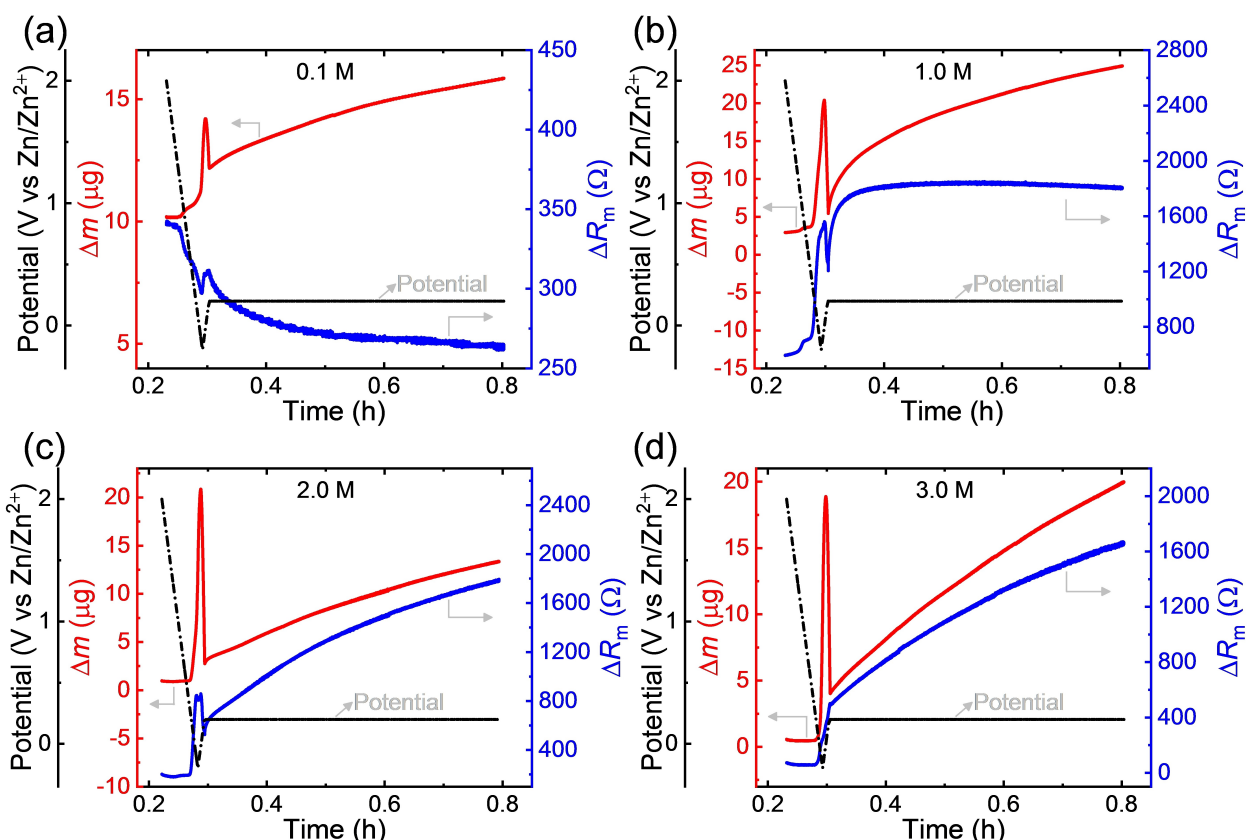


Figure 5. Detailed profiles of Δm and ΔR_m over time during the potential hold at 0.2 V vs Zn/Zn²⁺: in (a) 0.1 M, (b) 1.0 M, (c) 2.0 M, and (d) 3.0 M.

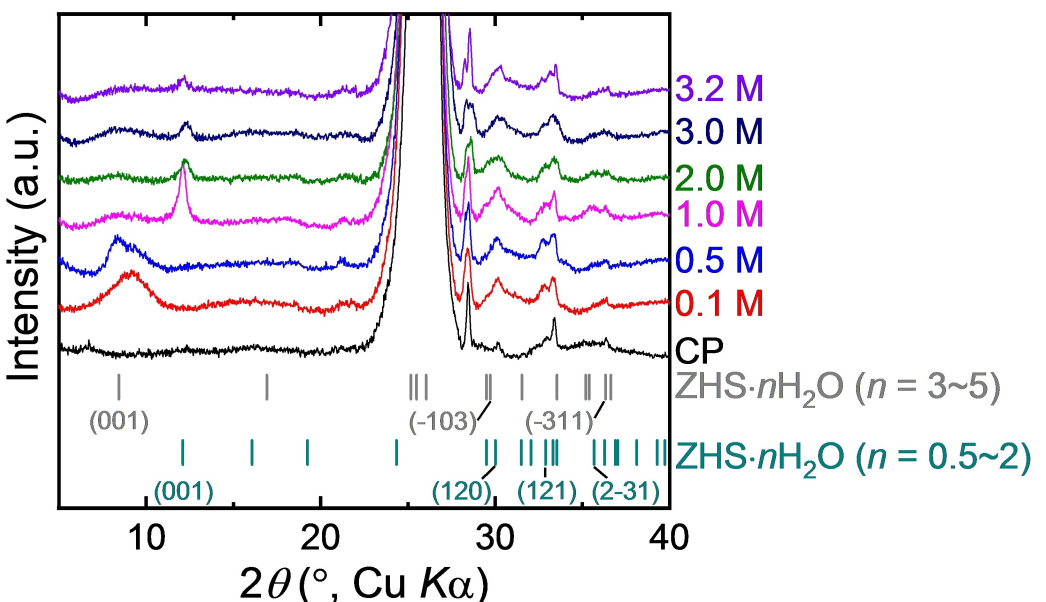


Figure 6. XRD analysis of the surface film on carbon paper (CP) substrates after holding the potential at 0.2 V vs Zn/Zn²⁺ for 30 min after the dissolution of deposited zinc in ZnSO₄ electrolytes with varied concentration. Here, ZHS stands for (Zn(OH)₂)₃(ZnSO₄) with different numbers of hydration.

is noteworthy that the hydration number of the ZHS byproduct decreased by increasing the concentration of electrolyte. Also, the remarkable reduction in the relative intensity of the (001) peak indicates substantially suppressed formation of ZHS at concentrations above 1.0 M; this means that highly concentrated electrolytes can alleviate the formation of ZHS on the surface. The minimal formation of ZHS with lower number of hydration may have affected enhanced coulombic efficiency and the reversible formation and decomposition of surface films at or above 1.0 M (Figure 2).

The composition and morphology of the surface film were further studied by Fourier-transform infrared (FT-IR) spectroscopy, scanning electron microscopy (SEM), and X-ray photo-electron spectroscopy (XPS) at varied potential in ZnSO₄ electrolyte with different concentrations. FT-IR spectra identified functional groups of O-H stretching (3000–3500 cm⁻¹) and SO₄²⁻ symmetric/asymmetric stretching (400–1120 cm⁻¹) in the surface film (Figure 7).^[36,37] XPS analysis of the O 1s, S 2p, and Zn 2p spectra revealed that the surface layer predominantly

consisted of zinc species in conjunction with SO₄²⁻ ions and O atoms (Figures S6–S8), in line with the FT-IR results.

After zinc deposition, platelets were observed on the surface and remained even after the zinc dissolution; such platelet morphology is the characteristics of ZHS (Figures 8 and S9–S12; Table S2).^[18,38] The EDS elemental mapping showed zinc, oxygen, and sulfur as the main components, supporting the presence of ZHS in the surface film (Figures S9–S12, Table S2).^[39] At 2.0 M or higher concentration, additional hexagonal aggregates were observed in addition to the platelets. Those aggregates can be correlated with remaining zinc salts that originated from the possible supersaturation in the highly concentrated electrolytes, or the less-hydrated ZHS that is observed in the XRD patterns. Conversely, the aggregates were not observable at 1.0 M or lower concentrations. These observations support the formation of fundamentally different surface films by the concentration of ZnSO₄ electrolytes, which provides insights toward the development of Zn-based aqueous batteries with enhanced stability by the

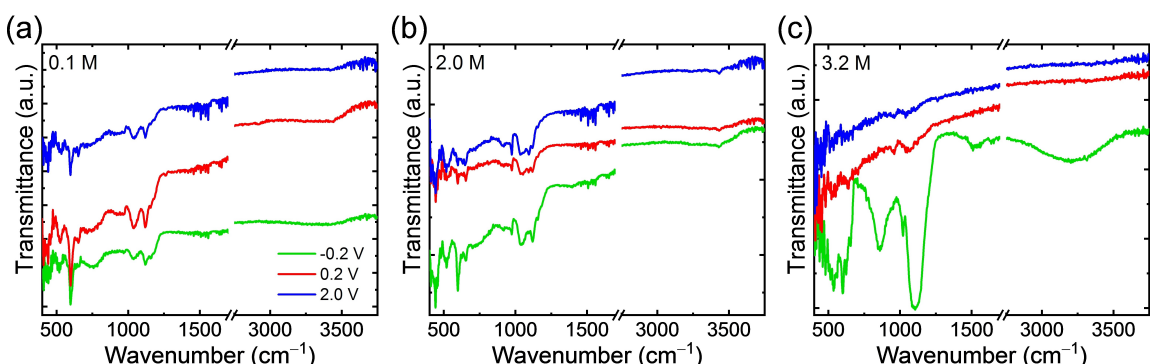


Figure 7. FT-IR analysis of the surface film: electrodes obtained at varied potential in (a) 0.1 M, (b) 2.0 M, and (c) 3.2 M ZnSO₄ electrolytes.

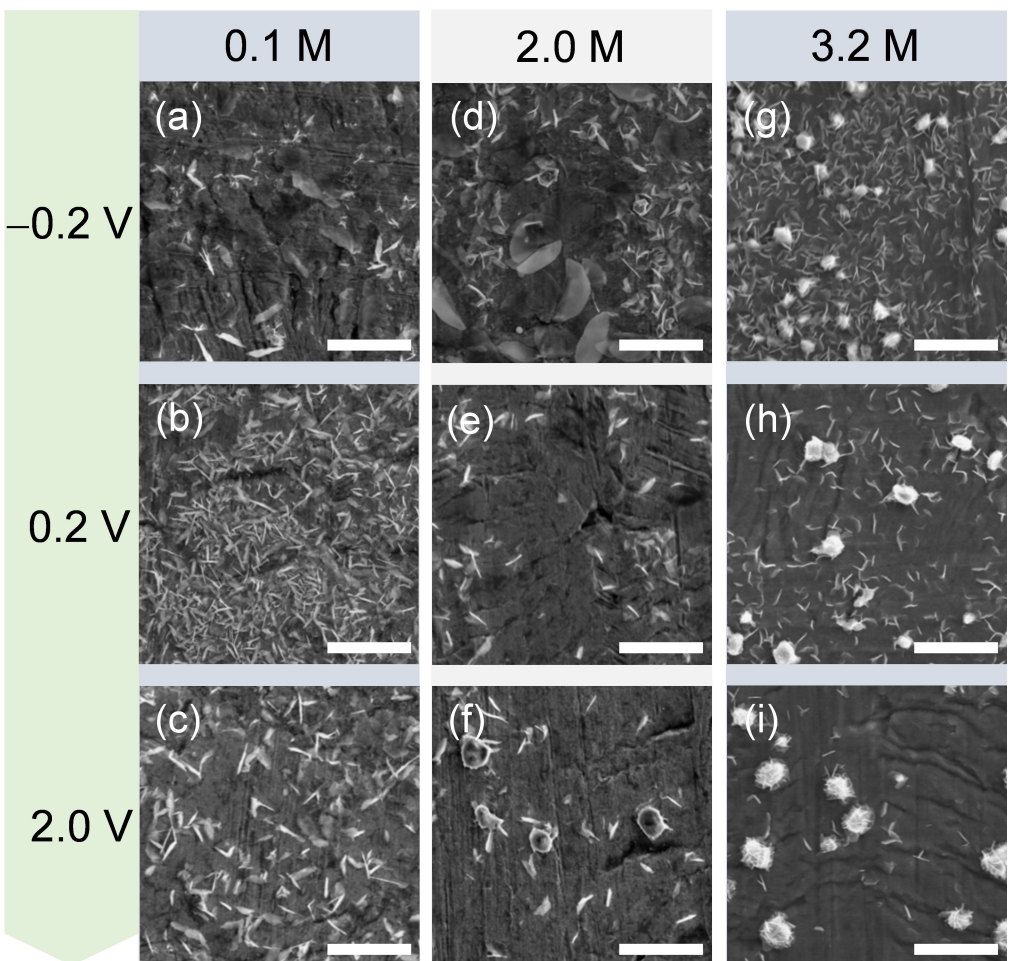


Figure 8. SEM images of electrodes obtained at varied potential: (a)-(c) 0.1 M, (d)-(e) 2.0 M, and (g)-(i) 3.2 M ZnSO_4 electrolytes, in the order of -0.2 V , 0.2 V , and 2.0 V vs Zn/Zn^{2+} . Scale bars equal to $5\text{ }\mu\text{m}$.

potential- and concentration-dependent passivation of zinc metal anodes.

Conclusions

EQCM analysis revealed the potential- and concentration-dependent formation and decomposition of surface films on zinc metal anode during the electrodeposition and dissolution of zinc in aqueous ZnSO_4 electrolytes for rechargeable zinc-ion batteries. Specifically, the changes in the motional resistance selectively reflected the amount and nature of the surface film, whereas the frequency change indicated the overall mass of both zinc metal and the surface film. The electrolyte concentration and the electrode potential were key factors that determined the characteristic reversibility, viscoelastic properties, and the composition of the resultant surface films. XRD analysis identified zinc hydroxyl sulfate as the dominant species in the surface films, with different number of hydration depending on the electrolytes' concentration. Among ZnSO_4 electrolytes with varied concentration, the electrolyte with a concentration of 2.0 M demonstrated nearly ideal mass per electrode

values during the zinc deposition-dissolution cycling. Furthermore, this concentration exhibited a remarkable coulombic efficiency of 96.5%, accompanied by maximum conductivity and deposition/dissolution currents. Likewise, the newly developed methodology based on complementary descriptors of Δm and ΔR_m provide crucial insights into the underlying interfacial processes on the zinc metal anode for the development of highly optimized zinc-based electrochemical systems.

Supporting Information

Supporting Information Available: a document containing additional figures and tables on the electrochemical and physico-chemical properties of the electrolyte and surface films.

Abbreviations

Electrochemical quartz crystal microbalance (EQCM)

Author Contributions

H.D.Y. designed the research; S.K.M., Y.O., E.S.K., K.S.M., H.J., and H.S.R. performed the sample preparation, characterization, and analysis; S.K.M. prepared the initial draft of manuscript, which was subsequently edited and reviewed by H.D.Y.; and everyone commented on the manuscript.

Acknowledgements

This research was supported by Korea Electric Power Corporation (Grant number: R22XO02-04). This research was also supported by Global-Learning & Academic research institution for Master's-PhD students, and Postdocs (LAMP) Program of the National Research Foundation of Korea (NRF) grant funded by the Ministry of Education (No. RS-2023-00301938).

Conflict of Interests

The authors declare no conflict of interest.

Data Availability Statement

The data that support the findings of this study are available from the corresponding author upon reasonable request.

Keywords: Zinc metal anode • Electrochemical quartz crystal microbalance (EQCM) • Surface films • Motional resistance • Electrochemistry

- [1] D. Chao, W. Zhou, F. Xie, C. Ye, H. Li, M. Jaroniec, S.-Z. Qiao, *Sci. Adv.* **2020**, *6*, eaba4098.
- [2] T. Liu, X. Cheng, H. Yu, H. Zhu, N. Peng, R. Zheng, J. Zhang, M. Shui, Y. Cui, J. Shu, *Energy Storage Mater.* **2019**, *18*, 68.
- [3] J. Liu, C. Xu, Z. Chen, S. Ni, Z. X. Shen, *Green Energy Environ.* **2018**, *3*, 20.
- [4] J. Shin, J. W. Choi, *Adv. Energy Mater.* **2020**, *10*, 2001386.
- [5] D. Kundu, B. D. Adams, V. Duffort, S. H. Vajargah, L. F. Nazar, *Nat. Energy* **2016**, *1*, 16119.
- [6] H. Pan, Y. Shao, P. Yan, Y. Cheng, K. S. Han, Z. Nie, C. Wang, J. Yang, X. Li, P. Bhattacharya, K. T. Mueller, J. Liu, *Nat. Energy* **2016**, *1*, 16039.
- [7] Y. Liu, X. Lu, F. Lai, T. Liu, P. R. Shearing, I. P. Parkin, G. He, D. J. L. Brett, *Joule* **2021**, *5*, 2845.
- [8] S. Mallick, C. R. Raj, *ChemSusChem* **2021**, *14*, 1987.

- [9] F. Wang, O. Borodin, T. Gao, X. Fan, W. Sun, F. Han, A. Faraone, J. A. Dura, K. Xu, C. Wang, *Nat. Mater.* **2018**, *17*, 543.
- [10] N. Zhang, X. Chen, M. Yu, Z. Niu, F. Cheng, J. Chen, *Chem. Soc. Rev.* **2020**, *49*, 4203.
- [11] A. R. Mainar, O. Leonet, M. Bengoechea, I. Boyano, I. de Meataz, A. Kvasha, A. Guerfi, J. Alberto Blázquez, *Int. J. Energy Res.* **2016**, *40*, 1032.
- [12] H. Li, S. Guo, H. Zhou, *Energy Storage Mater.* **2023**, *56*, 227.
- [13] T. Yamamoto, T. Shoji, *Inorg. Chim. Acta* **1986**, *117*, L27.
- [14] Y. Gui, Y. Lei, B. A. Fan, *Front. Chem.* **2020**, *8*, 827>.
- [15] K. Y. Kwon, T. H. Jo, J. S. Kim, F. Hasan, H. D. Yoo, *ACS Appl. Mater. Interfaces* **2020**, *12*, 42612.
- [16] W. Lu, C. Zhang, H. Zhang, X. Li, *ACS Energy Lett.* **2021**, *6*, 2765.
- [17] M. Zhou, S. Guo, G. Fang, H. Sun, X. Cao, J. Zhou, A. Pan, S. Liang, *J. Energy Chem.* **2021**, *55*, 549.
- [18] K. Y. Kwon, S. J. Kim, D.-M. Kim, H. Kim, S. K. Mohanty, K. T. Lee, H. D. Yoo, *Langmuir* **2021**, *37*, 13218.
- [19] E. L. Smith, J. C. Barron, A. P. Abbott, K. S. Ryder, *Anal. Chem.* **2009**, *81*, 8466.
- [20] H. Yang, K. Kwon, T. M. Devine, J. W. Evans, *J. Electrochem. Soc.* **2000**, *147*, 4399.
- [21] A. Cuenca, J. Agrisuelas, R. Catalán, J. J. García-Jareño, F. Vicente, *Langmuir* **2015**, *31*, 9655.
- [22] P. Lemaire, T. Dargon, D. Alves Dalla Corte, O. Sel, H. Perrot, J.-M. Tarascon, *Anal. Chem.* **2020**, *92*, 13803.
- [23] G. Sauerbrey, *Z. Phys.* **1959**, *155*, 206.
- [24] A. J. Bard, L. R. Faulkner, H. S. White, *Electrochemical Methods: Fundamentals and Applications*, John Wiley & Sons, Hoboken, New Jersey, 2022.
- [25] J. T. Matsushima, F. Trivinho-Strixino, E. C. Pereira, *Electrochim. Acta* **2006**, *51*, 1960.
- [26] J.-M. Kim, S.-M. Chang, H. Muramatsu, *Polymer* **1999**, *40*, 3291.
- [27] S. Na Songkhla, T. Nakamoto, *Chemosensors* **2021**, *9*, 9.
- [28] A. Bayaguud, Y. Fu, C. Zhu, *J. Energy Chem.* **2022**, *64*, 246.
- [29] M. K. Srinivasa, J. Lee, K. Hyun, H. D. Yoo, *ACS Appl. Mater. Interfaces* **2023**, *15*, 59296.
- [30] W. Zhang, X. Chen, Y. Wang, L. Wu, Y. Hu, *ACS Omega* **2020**, *5*, 22465.
- [31] C. Liu, X. Xie, B. Lu, J. Zhou, S. Liang, *ACS Energy Lett.* **2021**, *6*, 1015.
- [32] Z. Li, S. Ganapathy, Y. Xu, Z. Zhou, M. Sarilar, M. Wagemaker, *Adv. Energy Mater.* **2019**, *9*, 1900237.
- [33] X. Zhang, J. Li, D. Liu, M. Liu, T. Zhou, K. Qi, L. Shi, Y. Zhu, Y. Qian, *Energy Environ. Sci.* **2021**, *14*, 3120.
- [34] T. Staminirova, N. Petrova, G. Kirov, *J. Therm. Anal. Calorim.* **2016**, *125*, 85.
- [35] I. J. Bear, I. E. Grey, I. C. Madsen, I. E. Newnham, L. J. Rogers, *Acta Crystallogr. B* **1986**, *42*, 32.
- [36] A. Abu El-Fadl, I. C. Santos, A. Paulo, A. M. Nashaat, *Mater. Res. Express* **2018**, *5*, 066207.
- [37] T. H. Muster, I. S. Cole, *Corros. Sci.* **2004**, *46*, 2319.
- [38] W.-G. Lim, X. Li, D. Reed, *Small Methods* **2024**, *8*, 2300965.
- [39] X. Zhang, J. Zhang, N. Dai, Y. Yang, X. Yuan, F. Cao, J. Zhang, *Mater. Chem. Phys.* **2018**, *206*, 232.

Manuscript received: May 23, 2024

Revised manuscript received: July 16, 2024

Accepted manuscript online: July 17, 2024

Version of record online: September 9, 2024